

# Phase-dispersion light scattering for quantitative size-imaging of spherical scatterers\*

Tasshi Dennis, Shellee D. Dyer, and Andrew Dienstfrey

National Institute of Standards and Technology, 325 Broadway, Boulder, CO 80305  
email: [tasshi@boulder.nist.gov](mailto:tasshi@boulder.nist.gov), phone: 303-497-3507, FAX: 303-497-7621

## ABSTRACT

Using phase-dispersion spectra measured with optical coherence tomography (OCT) in the frequency domain, we demonstrated the quantitative sizing of multiple spherical scatterers on a surface. We modeled the light scattering as a slab-mode resonance and determined the size of the scatterers from a Fourier transform of the measured phase-dispersion spectra. Using a swept-source OCT system, we mapped the detected size of the scatters to the intensity of a two-dimensional surface image. The image was formed by raster-scanning a collimated beam of 200  $\mu\text{m}$  diameter across a sample with distinct size domains. The image shows a clear distinction between deposited polystyrene microspheres of 26 and 15  $\mu\text{m}$  average sizes. In a separate experiment, we demonstrated tissue-relevant sizing of scatterers as small as 5  $\mu\text{m}$  with a Fourier domain OCT system that utilized 280 nm of bandwidth from a super-continuum source. Our previous studies have demonstrated that the light scattered from a single sphere is, in general, non-minimum-phase; therefore, phase spectra can provide unique information about scattered light not available from intensity spectra alone. Also, measurements of phase spectra do not require background normalization to correct for the spectral shape of light sources or the spectral absorption of specimens. The results we report here continue our efforts towards combining intensity and phase spectra to enable improved quantitative analysis of complex tissue structures.

**Keywords:** dispersion, group delay, Mie scattering, optical coherence tomography, phase, spectral domain

## 1. INTRODUCTION

Light-scattering spectroscopy (LSS) has proven to be a powerful tool for the characterization of tissue morphology, and in particular for cancer screening based on the light scattering from the nuclei of epithelial cells<sup>1</sup>. Intensity scattering spectra as a function of wavelength<sup>1</sup> or angle<sup>2, 3</sup> can effectively determine nuclear size and index of refraction, with enlargement and densification of nuclei interpreted as one indication of dysplastic or cancerous samples. Normal cell nuclei have diameters between 4 and 7  $\mu\text{m}$ , while dysplastic nuclei might enlarge to as much as 20  $\mu\text{m}$ <sup>1</sup>. Optical coherence tomography is a powerful technique for depth-imaging of tissue *in vivo* by use of low-coherence interferometry<sup>4</sup>. It has been shown that LSS can be combined practically with OCT to provide depth-selectivity to scattered light<sup>5</sup>. To date, experimental efforts have focused on the measurement and analysis of intensity scattering spectra<sup>5, 6</sup>. However, we recently demonstrated that phase scattering spectra can also be used to determine the size and/or refractive index of scatterers<sup>7</sup>. In that work we discovered that even for the simplest case of a single scatterer the phase and intensity spectra are, in general, independent ("non-minimum-phase"). Therefore, each quantity must be measured independently, as neither can be inferred from the other. We expect this independence to hold for more complicated samples such as tissue, in which the scatterers are located at different depths within a volume. Therefore, the measurement of both phase and intensity more completely characterizes the scattering material. We anticipate that this characterization will, in turn, provide further insight into the health of the tissue. Additionally in reference 7, we presented a preliminary result for the phase scattering spectra from multiple scatterers, showing that a measurable signal indeed exists. Here we expand upon that result by demonstrating improved sizing resolution and the ability to quantitatively size-image scatterers on a surface from their phase spectra. We also demonstrate that phase measurements alone are advantageous because they do not require spectral normalization.

---

\* Contribution of an agency of the US government, not subject to copyright

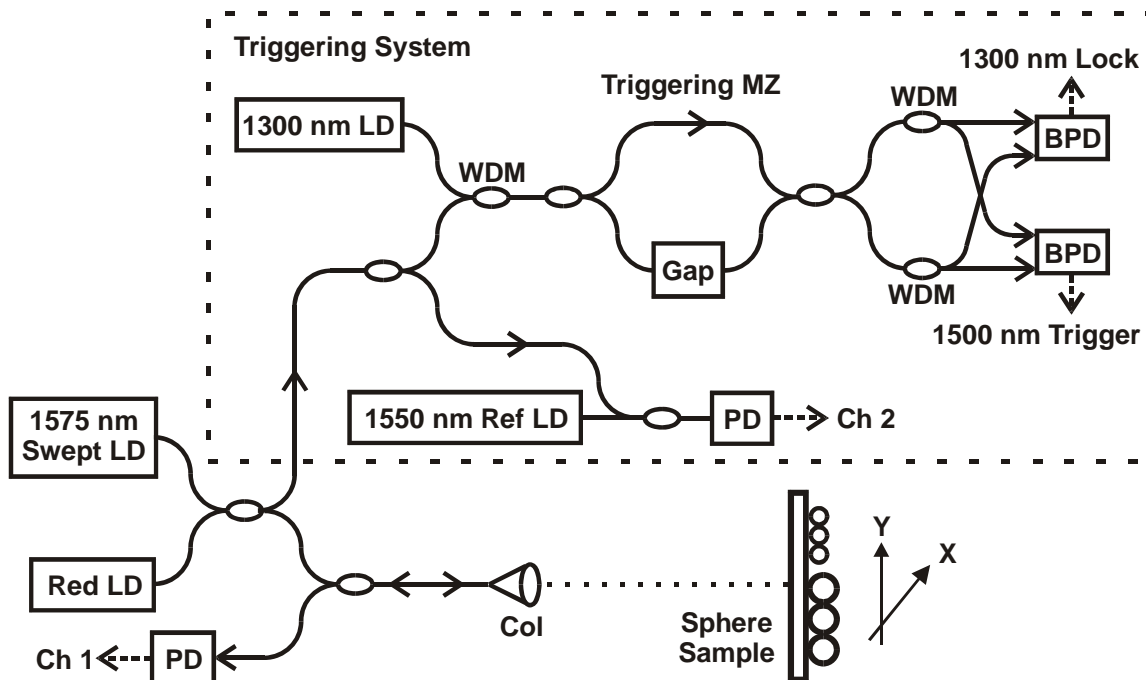


Fig. 1. Swept-source OCT phase-dispersion measurement system: LD, laser diode; PD, photodetector; BPD, balanced photodetector; WDM, 1300 / 1500 nm wavelength division multiplexer; MZ, Mach-Zehnder; Col, fiber collimator; Gap, adjustable air gap.

## 2. SWEEP-SOURCE OCT MEASUREMENTS

### 2.1 Experiment

Figure 1 illustrates the swept-source OCT system we used to collect phase-dispersion spectra and perform size-imaging. The light source was a commercial swept laser with a bandwidth of 112 nm centered at 1575 nm. The light from the swept laser was combined with a red alignment laser and launched into a single-mode fiber interferometer. A 200  $\mu\text{m}$  cylindrical beam was formed with a fiber collimator and directed onto a microscope slide covered with polystyrene microspheres on its back surface. The spheres were deposited from solution and dried naturally into hexagonally close-packed monolayers, with some spatial voids. A distinct sphere-size boundary was created by butting separate slides deposited with 15 and 26  $\mu\text{m}$  spheres. We used the front of the slide as the reference surface of a common-path interferometer, which provided excellent temporal stability and low material dispersion. The combination of back-scattered and reference light was detected with a photoreceiver and sampled with Channel 1 of an analog to digital (A/D) circuit board.

The dashed box of Figure 1 shows our drift-free system for uniform frequency triggering and absolute wavelength calibration for the samples of Channel 1. We used a Mach-Zehnder interferometer topology to create zero-crossing triggers from the balanced detection of interference fringes of the 1575 nm swept source. Wavelength division multiplexers and a second balanced photodetector were used to co-propagate and separately detect the light from a stabilized 1300 nm laser, which created an error signal to monitor drift. The trigger interferometer was stabilized by applying the error signal as feedback to the adjustable air-gap. The swept measurement laser was also combined with a stabilized reference laser at 1550 nm, resulting in a momentary beat-note signal on Channel 2 of the A/D board for coincident wavelengths. By knowing the exact frequency of one sample and the precise spacing between all samples, we were able to determine the absolute frequency of each sample of Channel 1.

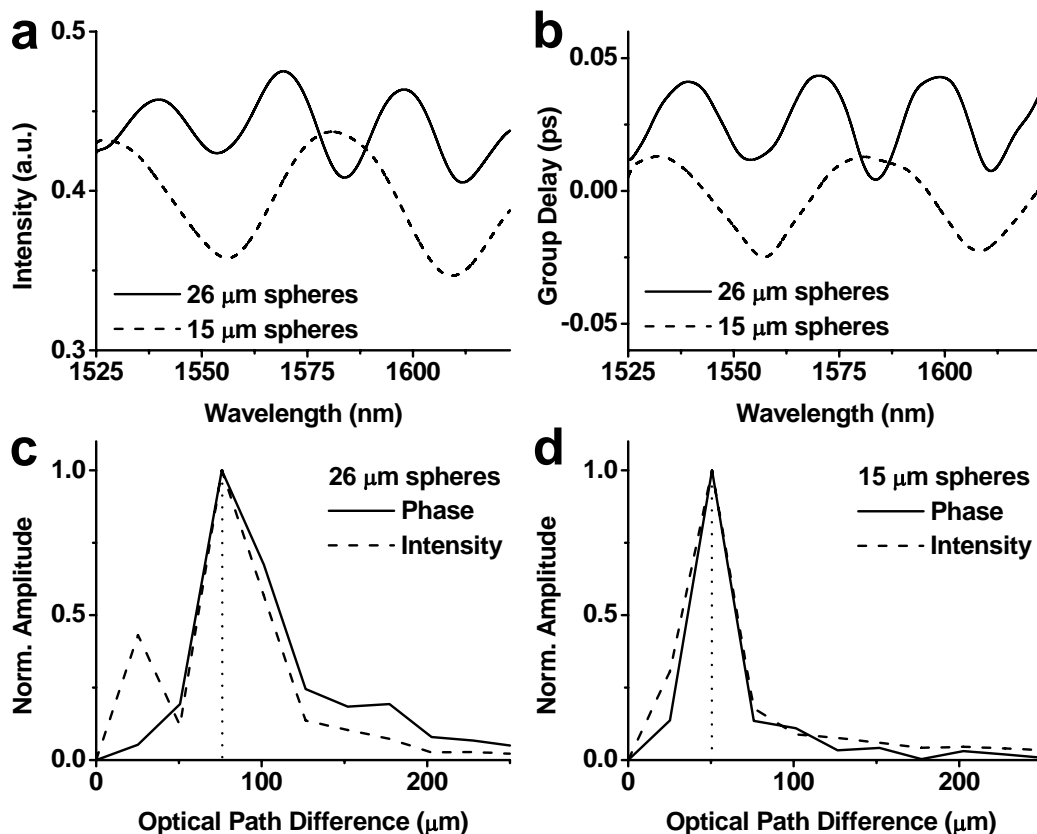


Fig. 2. (a) intensity and (b) phase scattering spectra for 15 and 26 μm polystyrene spheres measured with swept source OCT. The sizing distributions for polystyrene spheres of diameter (c) 26 μm and (d) 15 μm were determined by Fourier analysis of the intensity and phase spectra, shown respectively in Figures (a) and (b).

Our measurement technique was described in detail previously<sup>7</sup>, and involves using the method in reference 8 to calculate the group delay spectrum  $t_g(\omega)$  from the mirror-image-free complex impulse response. By computing the delay  $t_g(\omega)$  rather than the phase  $\phi(\omega)$ , where  $t_g(\omega) = d\phi(\omega)/d\omega$ , we avoided the linear phase term that results from defining the  $t = 0$  point of the impulse response. Additionally, the intensity scattering spectrum was calculated by conventional methods of low-coherence interferometry<sup>5</sup>.

## 2.2 Results

Figures 2a and 2b show measured intensity and phase scattering spectra, respectively, from regions with 26 and 15 μm spheres. For each sphere size the intensity and phase spectra show a strong correlation of fringe features, suggesting that over this particular wavelength range the scattering from multiple spheres of these sizes on a surface was minimum phase<sup>7</sup>. This is consistent with the notion that a minimum-phase system generates the strongest signal from the first reflecting surface<sup>9</sup>. However, in a volumetric geometry it is easy to envision that the dominant signal might originate from a group of scatterers distributed below the surface. The condition of minimum phase implies that one scattering spectrum could in principle have been predicted from the other by applying the Kramers-Kronig relation<sup>7</sup>. However, the intensity spectra contain slight background curvatures and slopes that we attribute to the spectral variation of the swept source and the measurement interferometer. By contrast, these variations are absent from the phase spectra.

We have observed as much as an order of magnitude reduction in the amplitude of phase and intensity fringes for scattering from multiple spheres, compared to the fringe amplitudes of spectra from a single sphere. We believe that the reduction is caused by speckle, from our observation that the fringe amplitudes increased in response to a decrease in both the number of spheres illuminated and the acceptance angle of the detection.

The size of the scatterers was determined by treating the spheres as etalons, dominated by slab-mode scattering<sup>6, 10</sup>, and applying a Fourier transform to the measured spectra to identify the dominant optical path differences (OPD). Here the  $OPD = 2nd$ , where  $n$  is the refractive index of the sphere and  $d$  is its diameter. Figures 2c and 2d show the distributions for the OPD of 26 and 15  $\mu\text{m}$  spheres, respectively, obtained from both the measured phase and intensity spectra. Based on the location of the peaks, the sphere diameters are calculated to be 24.0 and 16.0  $\mu\text{m}$ , assuming a refractive index of 1.58 for polystyrene. The diameters determined are in good agreement with the specified sizes of  $26 \pm 4 \mu\text{m}$  and  $15.5 \pm 0.9 \mu\text{m}$ , provided by the manufacturers of the microspheres.

We used this method for sizing spherical scatterers based on phase spectra to produce the size image shown in Figure 3 by raster scanning the sample across the measurement beam. The image covers a  $3 \text{ mm} \times 3 \text{ mm}$  area in  $200 \mu\text{m}$  steps, and shows a clear distinction between the regions containing 15 and 26  $\mu\text{m}$  spheres. Each measurement point shown was the result of spatially compounding four separate measurements ( $50 \mu\text{m}$  sub-steps in a square pattern) to reduce the effect of speckle. The OPD distributions from the four measurements were summed and the peak of the combined distribution was used to determine the average diameter. In the region of 15  $\mu\text{m}$  spheres, the measured diameter was consistently 16.0  $\mu\text{m}$ , with just a single measurement of 17.1  $\mu\text{m}$ . We attribute this one odd measurement to an incomplete sweep of the laser. In the region of 26  $\mu\text{m}$  spheres, the measured diameters are split between values of 24.0 and 32.0  $\mu\text{m}$ , due to the  $8 \mu\text{m}$  resolution of the system. The average measured size of the spheres in this region was 28  $\mu\text{m}$ , showing a slight disagreement with the specified size. We suspect that the disagreement is caused by speckle as well as an increase in the angular structure of the scattering as the size of the spheres increases<sup>2, 3</sup>.

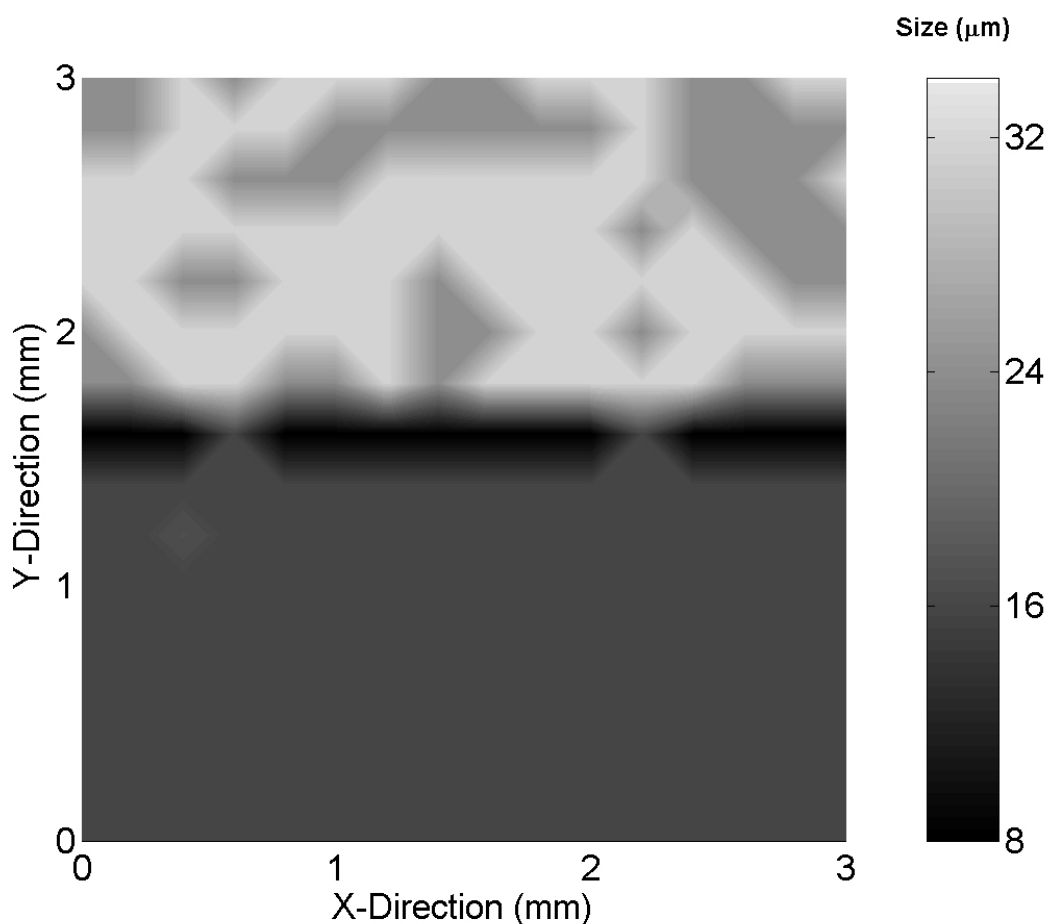


Fig. 3. Size image of a surface covered with microspheres of two distinct sizes: 26  $\mu\text{m}$  in the upper region and 15  $\mu\text{m}$  in the lower region. The intensity indicates sphere diameter, with a resolution of  $8 \mu\text{m}$ .

### 2.3 Discussion

While the intensity and phase spectra indicate the same peak OPD for each sphere size, the distributions themselves show slight differences. In particular, each distribution based on intensity contains more content at values of OPD below the peak location than the corresponding distributions based on phase. This is consistent with the observation that the intensity spectra of Fig. 2a show slight background curvatures, which can be difficult to remove in swept-source OCT measurements. This deleterious effect will have a greater impact on the ability to size smaller spheres, which generate weaker scattering signals and have broad spectral features that more closely resemble background variations.

In this demonstration the resolution of the spherical sizing was limited by the finite wavelength coverage of the spectra and the use of Fourier analysis to determine the dominant OPD. The spectra shown in Fig. 2 cover  $\Delta\lambda = 98$  nm, centered at  $\lambda_c = 1575$  nm. Because of edge effects from the signal processing<sup>7</sup>, this recovered bandwidth is smaller than the 112 nm bandwidth of the interferogram. Assuming that the spectral profile of the swept laser was ideally rectangular, the OPD was determined with a resolution of  $\lambda_c^2/\Delta\lambda = 25$   $\mu\text{m}$ . Treating the polystyrene spheres as etalons with a refractive index of 1.58 resulted in a sphere sizing resolution of 8  $\mu\text{m}$ . It is possible that improved resolution and sensitivity from the same measurement results could have been achieved by curve-fitting to predictions from Mie scattering theory. However, because closed-form solutions to Mie theory do not exist, approximations<sup>1</sup> or numerical tabulation approaches<sup>3</sup> are typically employed. We can also improve the resolution by increasing the spectral coverage of our measurements, as we will demonstrate in Section 3.

## 3. FOURIER DOMAIN OCT MEASUREMENTS

### 3.1 Experiment

To address the limited sizing resolution of our swept source OCT demonstration, we constructed a second, high-resolution measurement system based on a supercontinuum source, spectrograph, and photo-diode array. This Fourier-domain OCT system is illustrated in Fig. 4, and again utilized a sample measurement beam of 200  $\mu\text{m}$  in diameter. The ultra-broadband source was a commercially available nanosecond frequency comb with a low 25 kHz repetition frequency. Its spectrum was broadened in photonic crystal fiber to span from 575 to 2000 nm with a total output power of 135 mW. After filtering out visible wavelengths and coupling into single-mode fiber, we obtained roughly 10 mW of light in the 1200 to 1480 nm region for use in scattering measurements. The home-built spectrograph used a collimated incident beam of 9 mm in diameter, a 600 grooves/mm grating blazed at 1000 nm, and a spherical collection mirror with  $f = 150$  mm. The detector was an InGaAs linear array with 1024 elements covering the 280 nm measurement bandwidth. Each pixel was separated by 0.27 nm, resulting in a single-pass OCT depth range of about 1.7 mm in

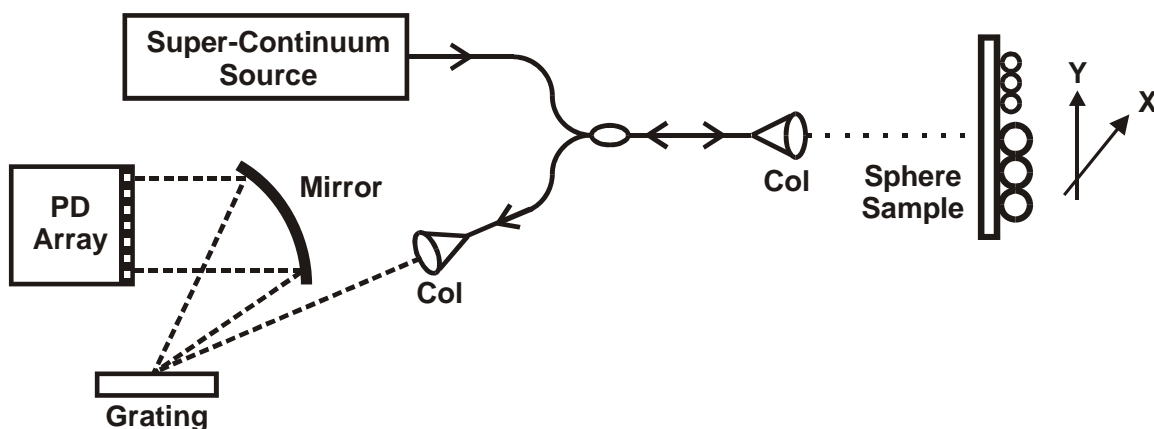


Fig. 4. Fourier-domain OCT system for phase-dispersion measurements: Col, collimator; PD, photo diode. The system was specifically designed to address the limited sizing resolution of the swept-source system shown in Fig. 1.

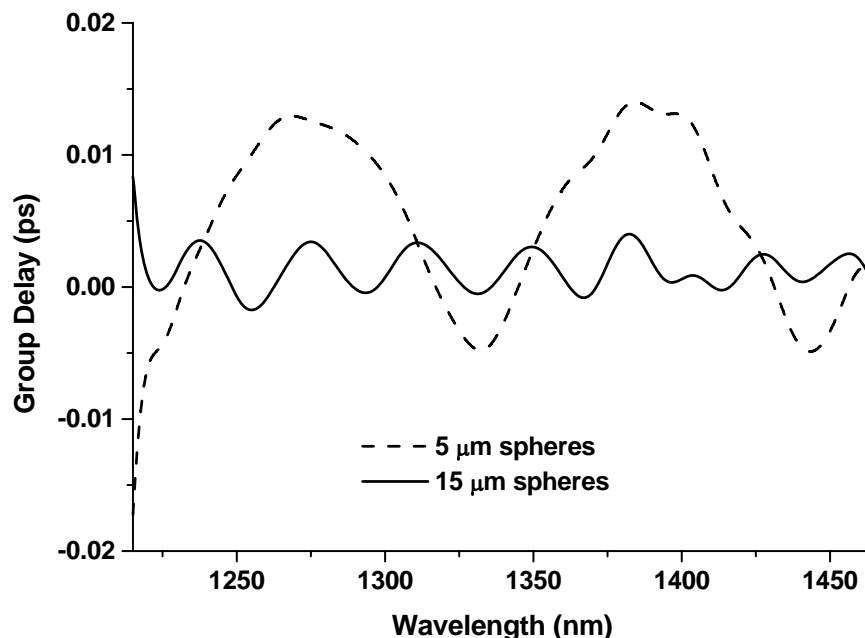


Fig. 5. Phase-dispersion spectra of 5 and 15  $\mu\text{m}$  spheres measured with Fourier domain OCT implemented with a supercontinuum source and spectrograph. As expected, the fringe period for 5  $\mu\text{m}$  spheres is about three times that of 15  $\mu\text{m}$  spheres.

vacuum. We illuminated about 6,200 grating lines in the spectrograph, resulting in a wavelength resolution of 0.21 nm, which was finer than the pixel spacing. Accurate wavelength calibration of the detector pixels was achieved by correlating the peak location of an incident tunable laser to the actual wavelength recorded by a wavelength meter.

### 3.2 Results

Figure 5 shows measured group delay spectra from monolayers of 5 and 15  $\mu\text{m}$  polystyrene spheres deposited on a glass cover slip of 150  $\mu\text{m}$  in thickness. The same signal processing conditions were applied to both spectra, resulting in clean fringe features with a wavelength resolution of 12 nm. By visual inspection, the period of the fringes for the 5  $\mu\text{m}$  spheres is about three times that of the 15  $\mu\text{m}$  spheres, as expected from the slab model. In many circumstances, especially for a single sphere, we might expect the height of the fringe features to increase as the diameter of the sphere increases. However, our results in Fig. 5 show just the opposite: the fringe amplitude for 5  $\mu\text{m}$  spheres is about four times that for 15  $\mu\text{m}$  spheres. We have not yet investigated this in detail, but we note that the same 200  $\mu\text{m}$  measurement beam illuminates about nine times more 5  $\mu\text{m}$  spheres than 15  $\mu\text{m}$  spheres.

The normalized OPD distributions for the group delay spectra of Fig. 5 are shown together in Fig. 6. The measured sphere sizes are calculated to be 4.5 and 15.9  $\mu\text{m}$ , assuming a refractive index of 1.58 for polystyrene. These results are in good agreement with the median sizes of  $5.0 \pm 0.38 \mu\text{m}$  and  $15.5 \pm 0.9 \mu\text{m}$  provided by the microsphere manufacturer. In contrast to the swept-source scattering measurements, the sizing interval of spheres has been reduced from 8  $\mu\text{m}$  to 2.3  $\mu\text{m}$ . Four discrete intervals separate the peaks for 5 and 15  $\mu\text{m}$  spheres in the distributions of Fig. 6.

### 3.3 Discussion

Based on measurements of the average size of multiple spheres of 5 and 15  $\mu\text{m}$  diameters, the broadband spectrometer OCT system has demonstrated tissue-relevant sizing of scatterers. Normal cell nuclei typically have diameters of about 5  $\mu\text{m}$ , while enlarged, pre-cancerous nuclei can be 15  $\mu\text{m}$  or larger. Even without the utilization of more optical bandwidth, the system has the potential for the intermediary sizing of scatterers due to a discrete sizing interval of just 2.3  $\mu\text{m}$ . As compared to our swept-source system, more subtle changes in tissue can now be detected, possibly at earlier stages of progression. We may also be able to study the light scattering of ellipsoidal particles, since real cell

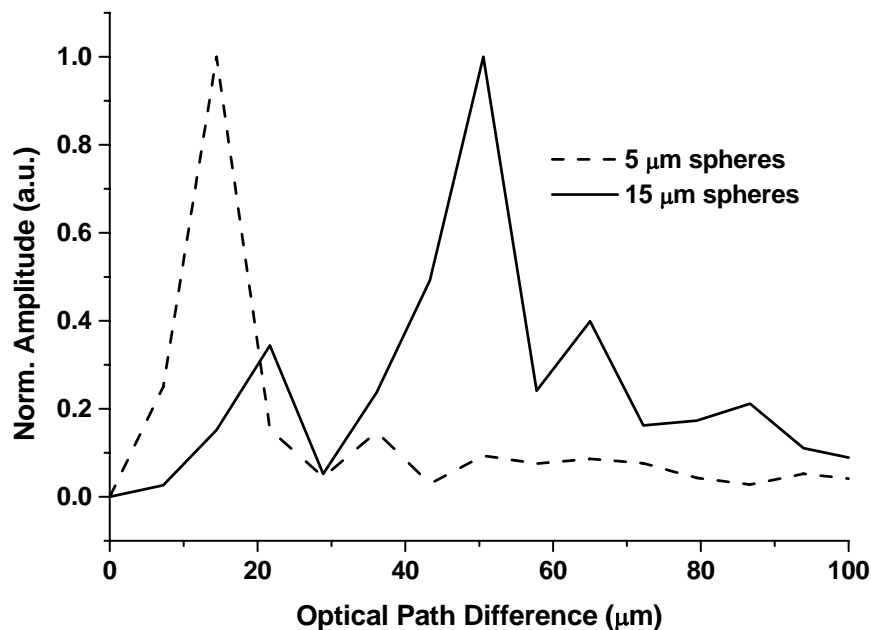


Fig. 6. The sizing distributions for the phase spectra shown in Fig. 5. The distinction between 5 and 15  $\mu\text{m}$  spheres is very clear, with 2.3  $\mu\text{m}$  sizing resolution.

nuclei are typically not perfect spheres. For practical experimental limitations, such as the finite number of array pixels, further improvements to sizing sensitivity and resolution may best be gained by implementing a more sophisticated spectral analysis based on Mie theory approximations and numerical tabulations<sup>1, 3</sup>. With slight improvements to automated operation, the broadband spectrometer OCT system can easily be adapted to raster scanning and the formation of size images such as Fig. 3.

#### 4. CONCLUSION

Our measurements have demonstrated with clear distinction the potential for using phase spectra to form images based on the size of spherical scatterers on a surface. We have also demonstrated that phase spectra do not require spectral normalization, which may be an advantage for weak signal measurements and for the sizing of small scatterers. Using a broadband measurement system, we have also demonstrated that the method is capable of tissue-relevant sizing. The high-resolution was achieved by use of a slab-mode resonance model, without resorting to the use of more complicated Mie theory models and analytic approximations.

Future investigations should consider more complicated, tissue-like samples composed of dense materials such as optical gels embedded with scatterers. The reduction in index contrast would result in weaker scattering signals, which would be more difficult to detect. Furthermore, the scatterers would be distributed throughout a volume, increasing the complexity of the speckle geometry and requiring greater utilization of the depth selectivity of OCT. In this situation we anticipate that a combination of information gathered from phase and intensity spectra would provide a more complete picture of the scatterers than a single spectral quantity. We expect that a combined measurement would go beyond simple nuclear sizing to the broader measurement of cell organization and tissue structure, which are other common indicators of tissue health. Furthermore, as illustrated by Adler et. al.<sup>11</sup>, spectral intensity modulation alone may not be able to distinguish a single large scatterer from many smaller scatterers in the same volume. A combination of phase and intensity spectra may be able to distinguish between these two disparate cases that otherwise appear degenerate. Both scattering cases are in general non-minimum-phase, and thus the phase spectrum, being related to but in general independent of the intensity spectrum, may provide the distinguishing information.

## REFERENCES

1. L.T. Perelman, V. Backman, M. Wallace, G. Zonios, R. Manoharan, A. Nusrat, S. Shields, M. Seiler, C. Lima, T. Hamano, I. Itzkan, J. Van Dam, J.M. Crawford, and M.S. Feld, "Observation of periodic fine structure in reflectance from biological tissue: a new technique for measuring nuclear size distribution," *Phys. Rev. Lett.* **80**, 627-630 (1998).
2. A. Wax, C.H. Yang, R.R. Dasari, and M.S. Feld, "Measurement of angular distributions by use of low-coherence interferometry for light-scattering spectroscopy," *Opt. Lett.* **26**, 322-324 (2001).
3. J. W. Pyhtila, R. N. Graf, and A. Wax, "Determining nuclear morphology using an improved angle-resolved low coherence interferometry system," *Opt. Express* **11**, 3473-3484 (2003).
4. A. F. Fercher, W. Drexler, C.K. Hitzenberger, and T. Lasser, "Optical coherence tomography – principles and applications," *Rep. Prog. Physics* **66**, 239-303 (2003).
5. A. Wax, C. Yang, and J. A. Izatt, "Fourier-domain low-coherence interferometry for light-scattering spectroscopy," *Opt. Lett.* **28**, 1230-1232 (2003).
6. R. N. Graf and A. Wax, "Nuclear morphology measurements using Fourier domain low coherence interferometry," *Opt. Express* **13**, 4693-4698 (2005).
7. S. D. Dyer, T. Dennis, L. K. Street, S. M. Etzel, T. A. Germer, and A. Dienstfrey, "Spectroscopic phase-dispersion optical coherence tomography measurements of scattering phantoms," *Opt. Express* **14**, 8138-8153 (2006).
8. V. Laude, "Noise analysis of the measurement of group delay in Fourier white-light interferometric cross correlation," *J. Opt. Soc. Am. B* **19**, 1001-1008 (2002).
9. A. Ozcan, M. J. F. Digonnet, and G. S. Kino, "Characterization of fiber Bragg gratings using spectral interferometry using minimum phase functions," *J. Lightwave Technol.* **24**, 1739 – 1757 (2006).
10. Y. Liu, X. Li, Y. L. Kim, and V. Backman, "Elastic backscattering spectroscopic microscopy," *Opt. Lett.* **30**, 2445-2447 (2005).
11. D. C. Adler, T. H. Ko, P. R. Herz, and J. G. Fujimoto, "Optical coherence tomography contrast enhancement using spectroscopic analysis with spectral autocorrelation," *Opt. Express* **12**, 5487-5501 (2004).